Journal of Alloys and Compounds 489 (2010) 504–508

Contents lists available at ScienceDirect

Journal of Alloys and Compounds

journal homepage: www.elsevier.com/locate/jallcom

Fabrication and optical properties of single-crystalline beta barium borate nanorods

Jiang Zhang*, Guiping He, Runhua Li, Xi Chen

Department of Physics, South China University of Technology, 381 Wushan Road, Guangzhou 510641, PR China

ARTICLE INFO

Article history:
Received 31 August 2009
Accepted 16 September 2009
Available online 25 September 2009

Keywords:
Nanostructure
Crystal growth
Optical properties
Scanning electron microscopy (SEM)
Transmission electron microscopy (TEM)

ABSTRACT

Single-crystalline beta barium borate (β-BaB_2O_4, β-BBO) nanorods with a diameter of 10–20 nm and a length up to several micrometers have been fabricated by a cetyltrimethyl ammonium bromide assisted hydrothermal method and subsequent annealing in air at 700 °C. Structure and composition characterizations were performed by X-ray powder diffraction, Fourier transform infrared spectra, Raman spectra and X-ray photoelectron spectra. The results indicate that β-BBO nanorods have an orthorhombic structure with space group of C_{3v}–$R3C$. Linear and nonlinear optical properties of β-BBO nanorods were examined by the absorption spectra, photoluminescence spectra and the powders second-harmonic generation measurement. The optical characterizations indicate that β-BBO nanorods are transparent from ultraviolet to the mid-infrared regions and exhibit a strong ultraviolet emission band at 382 nm. Compared with that of urea, higher second-harmonic generation conversion efficiency of β-BBO nanorods was measured. The possible growth process of β-BBO nanorods was also discussed briefly.

1. Introduction

In the past few years, one-dimensional (1D) nanostructures, such as nanorods, nanotubes and nanobelts, in a ternary borate system have been investigated by many groups [1–6]. However, most of studies were focused on the potential application in the mechanical filed for the manufacture of reinforcing composites [7–9] and lubrication additive [10]. Meanwhile, some of borate crystals have been studied extensively due to their unique nonlinear optical (NLO) and luminescent properties [11–14]. Among these borate NLO crystals, β-BaB_2O_4 (β-BBO) has many remarkable features, such as effective second-harmonic generation (SHG) coefficients up to six times higher than that of KH_2PO_4 (KDP) crystals, ability of generate a second-harmonic in the UV range, a wide transparency range and a high damage threshold [15–16]. Up to date, only a few efforts to fabricate 1D nanostructures of NLO materials have been reported. It has been reported by Magrez et al. that $KNbO_3$ nanorods can be synthesized by a hydrothermal route [17]. Highly anisotropic $KNbO_3$ nanocrystals in the form of nanoneedles and nanoplatelets were prepared by crystallization of the amorphous gel [18]. Using its SHG effect, an electrode-free, continuously tunable coherent visible light source compatible with physiological environments from an individual $KNbO_3$ nanowire was achieved by Nakayama et al. [19]. It indicates that 1D NLO nanostructures will have many potential applications in the range of physics, chemistry, materials science and biology. Perceptibly, further investigations of 1D NLO nanostructures should divert the attentions from $KNbO_3$ to the other NLO materials. Recently, β-BBO network-like nanostructures were synthesized by sol–gel approach and the reported SHG efficiency of the nanostructures is 78% relative to that of urea [20]. β-BBO nanospindles were also synthesized by an organic-free hydrothermal method [21].

In the present work, we reported that the fabrication of β-BBO nanorods with high crystallinity and uniform morphology by a cetyltrimethyl ammonium bromide (CTAB) assisted hydrothermal method and subsequent annealing in air at 700 °C. The investigations of the optical properties indicate that β-BBO nanorods are transparent from ultraviolet to the mid-infrared regions, and exhibit a strong ultraviolet emission band at 382 nm and display higher SHG conversion efficiency compared with that of urea.

2. Experimental

2.1. Preparation of materials

All of the chemicals were analytic-grade reagents used without further purification. Barium nitrate, sodium borohydride and CTAB were all purchased from Guangzhou Chemical Reagents Company. In a typical experiment, 0.005 mol $Ba(NO_3)_2$ and 0.01 mol $NaBH_4$ were dissolved in distilled water to make a 50 mL mixed solution with Ba:B ratio equal to 1:2. Then 10 mL 10% aqueous surfactant solution of CTAB was added to the mixture and the measured pH value of the mixture was about 11. The whole mixture was stirred for 30 min to form a homogeneous solution before it was transferred into a stainless steel autoclave, sealed, and maintained at 220 °C for 20 h. After the reaction, the suspension was cooled to room temperature naturally and the white suspended precipitate was filtered and washed repeatedly

* Corresponding author. Tel.: +86 20 87114127; fax: +86 20 87112837.
E-mail address: jonney@scut.edu.cn (J. Zhang).

0925-8388/$ – see front matter © 2009 Elsevier B.V. All rights reserved.
doi:10.1016/j.jallcom.2009.09.095

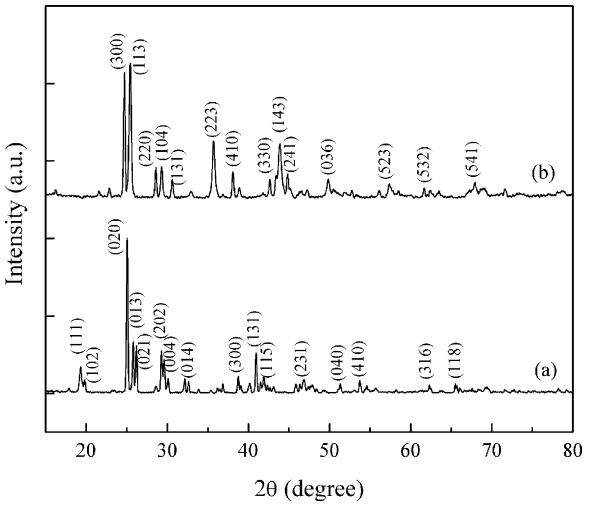

Fig. 1. XRD patterns of (a) the sample fabricated by the hydrothermal method at 220 °C and (b) the product annealed at 700 °C.

with distilled water and absolute ethanol. The obtained precipitate was annealed in a conventional tube furnace in air at 700 °C for 1 h, then ground to powders.

2.2. Characterization

The X-ray powder diffraction (XRD) patterns of the product were measured on a Rigaku D/max rA X-ray diffractometer equipped with graphite monochromatized high-intensity Cu Kα radiation (λ = 0.15418 nm) in the 2θ range 10–80°. The morphology of the product were observed by field-emission scanning electron microscopy (FE-SEM), which was carried out on a LEO 1530 VP FE-SEM operated at an acceleration voltage of 5 kV. The microstructure of the product were observed by transmission electron microscopy (TEM) and high-resolution transmission electron microscopy (HRTEM) images, which were performed on a Philips CM300 transmission electron microscope with an acceleration voltage of 200 kV. The Fourier transform infrared (FTIR) spectra were recorded as KBr discs on a Perkin-Elmer BX-II spectrometer in the range of 400–4000 cm^{-1}. The Raman spectra were recorded on a HJY LabRAM Aramis Raman microspectroscope with a 532 nm laser as an excita-

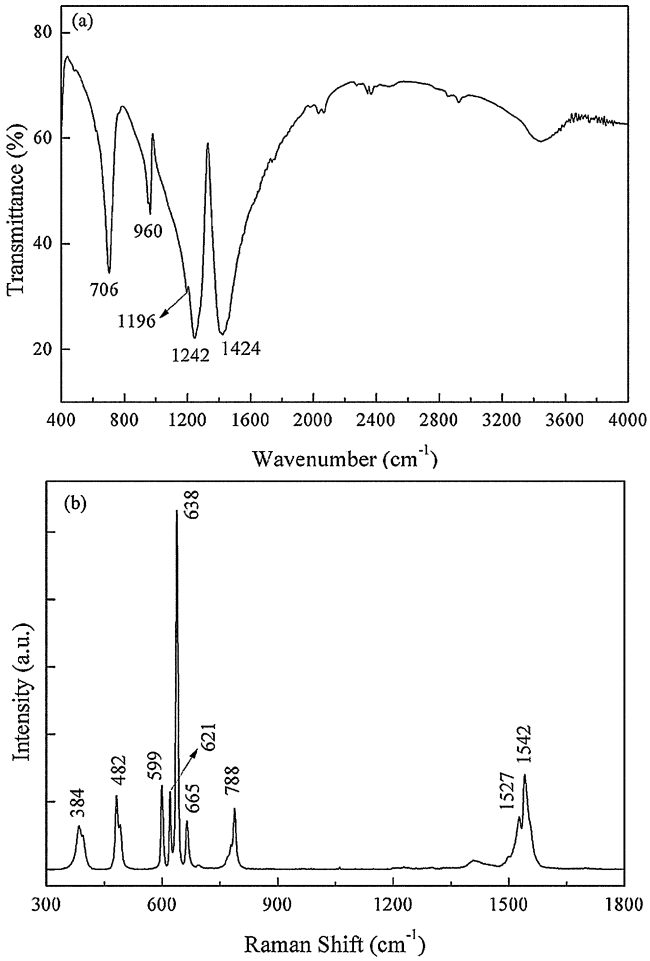

Fig. 3. (a) FTIR and (b) Raman spectra of β-BBO nanorods.

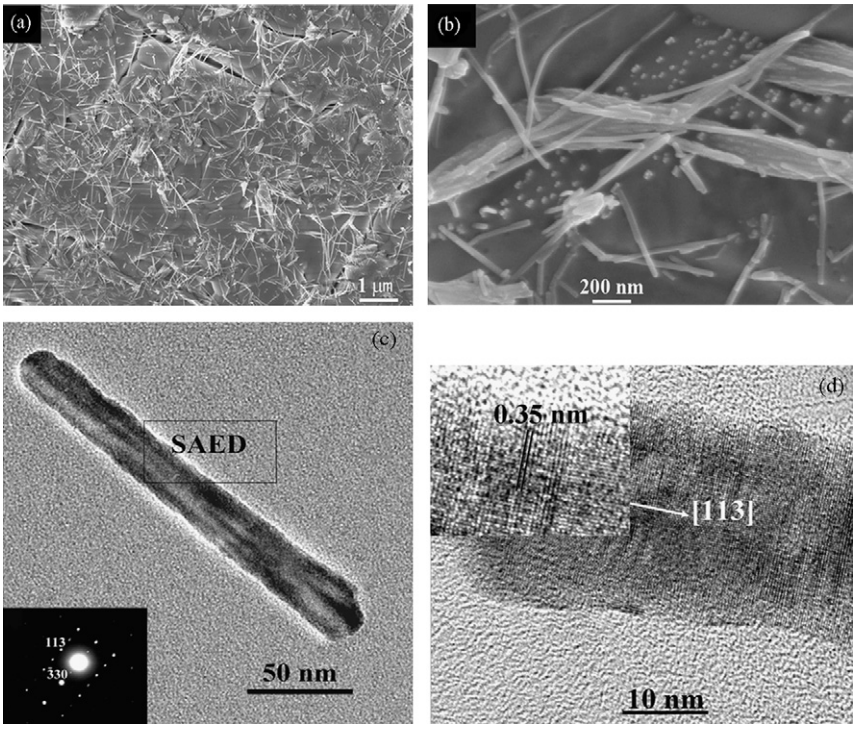

Fig. 2. (a) Low- and (b) high-magnification SEM images of β-BBO nanorods; (c) typical TEM image of an individual β-BBO nanorod, inset is corresponding SAED pattern; (d) HRTEM image of the nanorod.

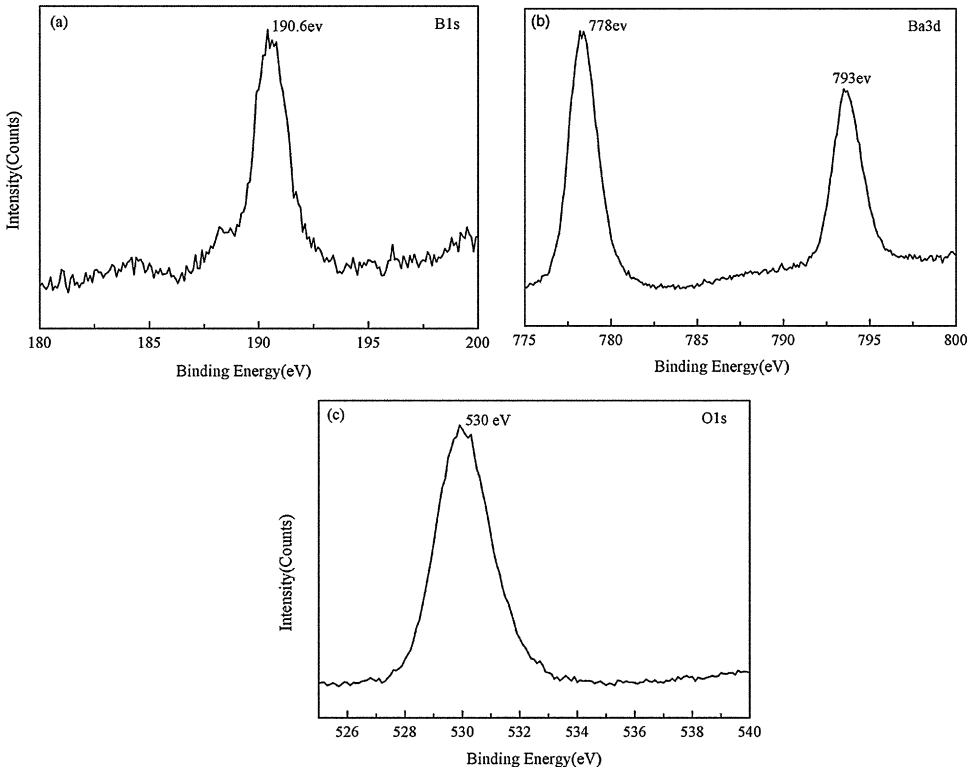

Fig. 4. High-resolution XPS spectra of (a) B 1s region; (b) Ba 3d region; (c) O 1s region for β-BBO nanorods, respectively.

tion source. X-ray photoelectron spectra (XPS) were measured on a Kratos AXis Ultra (DLD) photoelectron spectrometer, using Al Kα ($h\nu$ = 1486.69 eV) as the excitation source and choosing C 1s (284.6 eV) as the reference line. UV–vis–NIR absorption spectra were characterized by a Shimadzu UV-3150 spectrophotometer. The room-temperature photoluminescence (PL) spectra were measured on a Perkin-Elmer LS-55 luminescence spectrometer with a Xe lamp as the excitation source. The excitation wavelength used in the PL measurement was 250 nm. NLO properties were measured by Kurtz powder SHG method. A Q-switched mode-locked Nd:YAG laser (λ = 1064 nm) with 12 ns pulse width and 5 Hz repetition rate was used as a illuminating source. The signals were detected by means of photomultiplier tube connected to a 250 MHz digital storage oscilloscope (Good Will, GDS-840C).

3. Results and discussion

3.1. Structure and composition characterizations

Fig. 1a shows a representative XRD pattern of the sample prepared by the hydrothermal method at 220 °C for 20 h. All the peaks can be indexed to monoclinic phase of barium polyborate ($Ba_3B_6O_9(OH)_6$) (JCPDS 01-071-2501) with lattice parameter of a = 0.699, b = 0.714 and c = 1.192 nm. Fig. 1b shows the XRD pattern of the product obtained after annealing at 700 °C in air for 1 h. All the peaks can be indexed to orthorhombic phase of β-BBO (JCPDS 80-1489) with lattice constants of a = 1.253 and c = 1.272 nm. No characteristic peaks were observed for any impurities. The strongest diffraction peak of the sample was located at 2θ = 25.44°, the corresponding plane was (1 3 1), and the d spacing was 0.35 nm.

Fig. 2a is a low-magnification SEM image of the annealed product and it can be seen that a large quantity of β-BBO nanorods was obtained by this approach. The high-magnification SEM image (Fig. 2b) shows that these nanorods have a good uniform diameter of 10–20 nm and length of several micrometers. In order to investigate more details of the structure and morphology of β-BBO nanorods, TEM and HRTEM observations were carried out consequently. Fig. 2c shows a typical TEM image of an individual β-BBO nanorod lying on the copper grid. The TEM observation displays that the nanorods have a uniform structure and a diameter range similar to that observed by SEM. The inset in Fig. 2c is corresponding select electron diffraction (SAED) pattern of the nanorod, which can be indexed to indexed to the (1 1 3) and ($\bar{3}$ 3 0) planes of the orthorhombic structure of β-BBO, respectively. Fig. 2d illustrates the lattice-resolved HRTEM image of the nanorod and the clear lattice fringes exhibit good crystallinity of β-BBO nanorods. The inset shows enlarged image indicating the lattice spacing is about 0.35 nm, which corresponds to the (1 1 3) crystalline plane of β-BBO. Both the HRTEM image and SAED pattern indicate that the β-BBO nanorods are single-crystalline structure. In addition, our observations also show that the growth of β-BBO nanorod is along the [1 1 3] direction.

The β-BBO crystal is built up by the Ba^{2+} cations and the $(B_3O_6)^{3-}$ anions rings by turns. The phase structure of β-BBO belongs to space group of C_{3v}–$R3C$. The FTIR spectrum of β-BBO nanorods is shown in Fig. 3a. The frequencies range from 1100 and 1300 cm^{-1} can be assigned to the characteristic for the B–O stretching mode in the $(BO_3)^{3-}$ unit, which is the component of the $(B_3O_6)^{3-}$ ring [22]. The strong absorption bands observed close to at 706 cm^{-1} are due to O–B–O bending vibrations of the same unit. The absorption peaks at 960 and 1424 cm^{-1} result from the stretching vibration of extra-ring B–O bonds. Fig. 3b shows the Raman spectrum of β-BBO nanorods. The assignment of the Raman vibration modes observed in our sample was based on the Raman data reported by Ney et al. for β-BBO single crystal [23]. The peaks at 1542, 1527, 788, 638, and 599 cm^{-1} can be attributed to transversal-optical (TO) photon mode, and the peaks at 665, 621, 482, and 384 cm^{-1} can be assigned to longitudinal-optical (LO) photon mode. The FTIR and Raman spectra indicate that β-BBO nanorods have the structure characteristics of bulk β-BBO crystals.

The XPS measurements were carried out to further investigate the chemical composition and state of β-BBO nanorods. Fig. 4 shows the high-resolution XPS spectra of the B 1s, Ba 3d and O 1s region, respectively. According to the reported studies [24], the peaks can

be attributed to the binding energy of B 1s, Ba 3d and O 1s as follow. Due to the low cross-section of the B 1s core level, the XPS line intensity is quite low. In Fig. 4a, the B 1s core level spectrum recorded under higher sensitivity is reproduced. The peak at 190.6 eV indicates that B 1s of β-BBO. As shown in Fig. 4b, the first peak at 778 eV can be attributed to Ba $3d_{5/2}$ and the second peak at 793 eV corresponds to Ba $3d_{3/2}$. The presence of the 530 eV peak for O 1s (Fig. 4c) and the 778 eV peak for Ba $3d_{5/2}$ in the XPS spectra recorded clearly suggest the presence of Ba–O [25], which is consistent with β-BBO crystal structure.

3.2. Growth of β-BBO nanorods

The chemical reactions for the formation of β-BBO nanorods may be considered as below. Firstly, in the hydrothermal treatment process, $Ba_3B_6O_9(OH)_6$ will precipitate according to the reactions (1) and (2). As shown in the literature [21,25], $Ba_3B_6O_9(OH)_6$ can be dehydrated consequently to form β-BBO according to reaction (3):

$$NaBH_4 + 2H_2O \rightarrow NaBO_2 + 4H_2\uparrow \quad (1)$$

$$6BO_2^- + 3Ba^{2+} + 3H_2O \rightarrow Ba_3B_6O_9(OH)_6\downarrow \quad (2)$$

$$Ba_3B_6O_{10}(OH)_6 \xrightarrow{700\ ^\circ C} \beta\text{-}BaB_2O_4 + 3H_2O \quad (3)$$

We think that the CTAB surfactant plays an important role to the fabrication of structurally uniform β-BBO nanorods. CTAB has been widely used as a soft template for the formation 1D nanostructures as well as stabilizing the 1D nanostructures, because it can form an elongated rod-like micelle structure and the function between CTAB and each crystal plane of participated nanocrystals is different [26–28]. When the solution of CTAB is added and stirred with mixed solution of $Ba(NO_3)_2$ and $NaBH_4$, electrostatic interaction between CTA^+ and BO_2^- are formed. Thus CTAB can selectively adsorb to the surfaces of newly nucleated nanoparticles and prevents other colloids from attaching to the nanoparticles. As a result, the growth rate of the nanoparticle in some certain direction will be confined and a special direction is kept as the preferential growth orientation [27]. Thus CTAB acts as a molecule-direction template for the growth of nanorods. During the following hydrothermal treatment, nanorods can grow along the chain of CTAB. After dehydrating $Ba_3B_6O_9(OH)_6$ precipitates, β-BBO nanorods was formed. It should be noted that some of nanorods aggregated to form arrays (as shown in Fig. 2b), which may be due to the interaction of the organic molecules of CTAB coated on the nanorods.

3.3. Optical properties

Fig. 5a shows the UV–vis–NIR absorption spectrum of β-BBO nanorods dispersed in ethanol. It can be seen that β-BBO nanorods have no obvious absorption edge in the range of 200–2000 nm, which is in consistent with the data for β-BBO single crystal [15]. Since β-BBO is an attractive photoluminescent material, PL measurement was investigated. The room-temperature PL spectrum of the β-BBO nanorods under photon excitation of 250 nm is shown in Fig. 5b. A strong emission bands at 382 nm (approx. 3.25 eV) were observed, which can be attributed to self-trapped exaction-type excitations localized in the crystal defects (vacancies) [29].

Kurtz powder SHG measurement is an extremely useful method for initial testing of materials for second-harmonic generation. The SHG intensity of the sample compared with that of the reference was used to determine the capability of the second-order nonlinear optical effects [30]. In our studies, urea with the particle sizes of 40 μm was used as the reference sample. The SHG signal generated in the sample was confirmed from emission of green radiation. As shown in Fig. 6, the SHG measurement indicates that the SHG conversion efficiency of β-BBO nanorods is greater than that of urea. The measured SHG intensity of β-BBO nanorods is about 1.2 times that of urea and also greater than that of β-BBO network-like nanostructures. As described previously [31,32], it was conceived that the length, diameter and ordering degree of the nanorods have an important effect on their NLO properties. We suggest that higher SHG conversion efficiency of β-BBO nanorods may be related with high crystallinity and assembly of the nanorods. Furthermore, in-depth studies on the synthesis of β-BBO nanorods arrays and the relations between the structures and their NLO properties are under way.

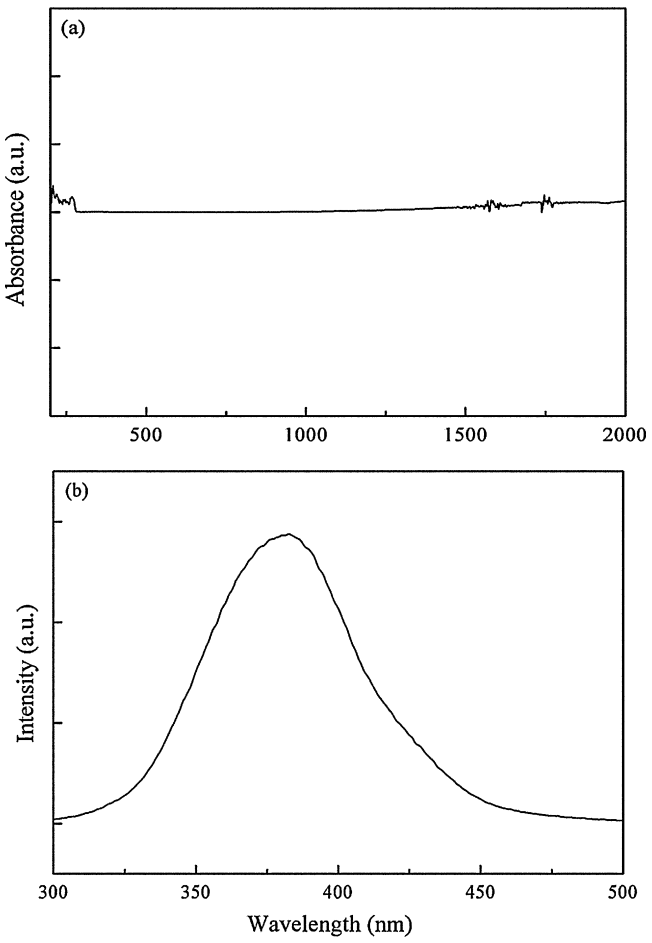

Fig. 5. (a) UV–vis–NIR absorption and (b) PL spectra of β-BBO nanorods.

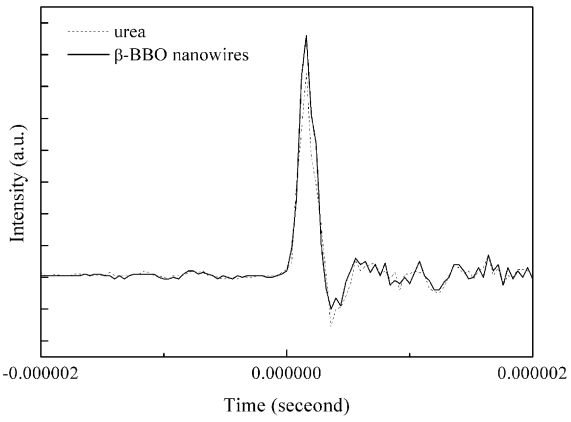

Fig. 6. Temporal profiles of SHG response of β-BBO nanorods compared with that of urea.

4. Conclusion

In summary, single-crystalline β-BBO nanorods with uniform structure have been fabricated by a CTAB assisted hydrothermal method and subsequent annealing. Investigations of the optical properties of β-BBO nanorods indicate that these nanostructures are transparent in the range of 200–2000 nm and show a strong UV emission. The SHG intensity of β-BBO nanorods is about 1.2 times that of urea. These nanorods are expected to exhibit potential application in the nano-optical device and used as doublers for ultrashort laser pulses. It is also believed that this approach can be extended to the fabrication of other 1D NLO nanostructures given that appropriate reaction conditions can be found.

Acknowledgements

The financial support from the Natural Science Foundation of Guangdong Province (Grant No. 6050980) and the National Natural Science Foundation of China (Grant No. 10704026) are greatly acknowledged.

References

[1] C. Cheng, C. Tang, X.X. Ding, X.T. Huang, Z.X. Huang, S.R. Qi, L. Hu, Y.X. Li, Chem. Phys. Lett. 373 (2003) 626.
[2] Y. Li, Z.Y. Fan, J.G. Lu, R.P.H. Chang, Chem. Mater. 16 (2004) 2512.
[3] Y. Li, R.P.H. Chang, Mater. Chem. Phys. 97 (2006) 23.
[4] C.C. Tang, E.M. Elssfah, J. Zhang, D.F. Chen, Nanotechnology 17 (2006) 2362.
[5] J. Zhang, Z.Q. Li, B. Zhang, Mater. Chem. Phys. 98 (2006) 195.
[6] E.M. Elssfah, H.S. Song, C.C. Tang, J. Zhang, X.X. Ding, S.R. Qi, Mater. Chem. Phys. 101 (2007) 499.
[7] X.Y. Tao, X.N. Wang, X.D. Li, Nano Lett. 7 (2007) 3172.
[8] X.X. Zhang, C.F. Deng, Y.B. Shen, D.Z. Wang, L. Geng, Mater. Lett. 61 (2007) 35046.
[9] X.Y. Tao, X.D. Li, Nano Lett. 8 (2008) 505.
[10] Y. Zeng, H.B. Yang, W.Y. Fu, L. Qiao, L.X. Chang, J.J. Chen, H.Y. Zhu, M.H. Li, G.T. Zou, Mater. Res. Bull. 43 (2008) 2239.
[11] C.T. Chen, Y.C. Wu, A.D. Jiang, B.C. Wu, G.M. You, S.J. Lin, J. Opt. Soc. Am. B 6 (1989) 616.
[12] W.G. Zou, M.K. Lu, F. Gu, S.F. Wang, Z.L. Xiu, G.J. Zhou, Mater. Sci. Eng. B 127 (2006) 134.
[13] J.F. Liu, X.M. He, C.T. Xia, G.Q. Zhou, S.M. Zhou, J. Xu, W. Yao, L.J. Qian, Thin Solid Films 510 (2006) 251.
[14] R. Bhatt, S. Ganesamoorthy, I. Bhaumik, A.K. Karnal, V.K. Wadhawan, Opt. Mater. 29 (2007) 801.
[15] D. Eimerl, L. Davis, S. Velsko, E.K. Graham, A. Zalkin, J. Appl. Phys. 62 (1987) 1968.
[16] D. Nikogosyan, Appl. Phys. A: Mater. Sci. Process. 52 (1991) 359.
[17] A. Magrez, E. Vasco, J.W. Seo, C. Dieker, N. Setter, L. Forro, J. Phys. Chem. B 110 (2006) 58.
[18] I. Pribošič, D. Makovec, M. Drofenik, Chem. Mater. 17 (2005) 2953.
[19] Y. Nakayama, P.J. Pauzauskie, A. Radenovic, R.M. Onorato, R.J. Saykally, J. Liphardt, P.D. Yang, Nature 447 (2007) 1098.
[20] Q.R. Zhao, X. Zhu, X. Bai, H.H. Fan, Y. Xie, Eur. J. Inorg. Chem. (2007) 1829.
[21] R. Li, X.Y. Tao, X.D. Li, J. Mater. Chem. 19 (2009) 983.
[22] U. Moryc, W.S. Ptak, J. Mol. Struct. 511–512 (1999) 241.
[23] P. Neyy, M.D. Fontanay, A. Maillardy, K. Polgárz, J. Phys.: Condens. Matter 10 (1998) 673.
[24] S.C. Sabharwal, Sangeeta, M. Goswami, S.K. Kulkarni, B.D. Padalia, J. Mater. Sci. 11 (2000) 325.
[25] Y.F. Zhou, M.C. Hong, Y.Q. Xu, B.Q. Chen, C.Z. Chen, Y.S. Wang, J. Cryst. Growth 276 (2005) 478.
[26] X.M. Sun, X. Chen, Z.X. Deng, Y.D. Li, Mater. Chem. Phys. 78 (2003) 99.
[27] M.H. Chen, L. Gao, J. Am. Ceram. Soc. 88 (2005) 1643.
[28] G.C. Xi, Y.K. Liu, X.Q. Wang, X.Y. Liu, Y.Y. Peng, Y.T. Qian, Cryst. Growth Des. 6 (2006) 2567.
[29] V. Kisand, R. Kink, M. Kink, J. Maksimov, M. Kirm, I. Martinson, Phys. Scr. 54 (1996) 542.
[30] S.P. Chou, D.J. Sun, H.C. Lin, P.K. Yang, Chem. Commun. 9 (1996) 1045.
[31] J.C. Johnson, K.P. Knutsen, H. Yan, M. Law, Y.F. Zhang, P.D. Yang, R.J. Saykally, Nano Lett. 2 (2002) 279.
[32] S.K. Das, M. Bock, C. O'Neill, R. Grunwald, K.M. Lee, H.W. Lee, S. Lee, F. Rotermund, Appl. Phys. Lett. 93 (2008) 181112.